Evolution of Eu valence and superconductivity in layered $Eu_{0.5}La_{0.5}FBiS_{2-x}Se_x$ system

Y. Mizuguchi,[1] E. Paris,[2] T. Wakita,[3] G. Jinno,[1] A. Puri,[4] K. Terashima,[3] B. Joseph,[5] O. Miura,[1] T. Yokoya,[3] and N. L. Saini[2]

[1]*Department of Electrical and Electronic Engineering, Tokyo Metropolitan University, 1-1 Minami-osawa, Hachioji, Tokyo, 192-0397, Japan*

[2]*Dipartimento di Fisica, Universitá di Roma "La Sapienza," Piazzale le Aldo Moro 2, 00185 Rome, Italy*

[3]*Research Institute for Interdisciplinary Science, Okayama University, Okayama 700-8530, Japan*

[4]*CRG-LISA, ESRF, 71 avenue des Martyrs, 38000 Grenoble, France*

[5]*Elettra, Sincrotrone Trieste, Strada Statale 14, Km 163.5, Basovizza, 34149 Trieste, Italy*

(Received 1 December 2016; revised manuscript received 25 January 2017; published 27 February 2017)

We have studied the effect of Se substitution on Eu valence in a layered $Eu_{0.5}La_{0.5}FBiS_{2-x}Se_x$ superconductor using a combined analysis of x-ray absorption near-edge structure (XANES) and x-ray photoelectron spectroscopy (XPS) measurements. Eu L_3-edge XANES spectra reveal that Eu is in the mixed valence state with coexisting Eu^{2+} and Eu^{3+}. The average Eu valence decreases sharply from ~2.3 for $x = 0.0$ to ~2.1 for $x = 0.4$. Consistently, Eu $3d$ XPS shows a clear decrease in the average valence by Se substitution. Bi $4f$ XPS indicates that effective charge carriers in the $BiCh_2$ (Ch = S, Se) layers are slightly increased by Se substitution. On the basis of the present results it has been discussed that the metallic character induced by Se substitution in $Eu_{0.5}La_{0.5}FBiS_{2-x}Se_x$ is likely to be due to increased in-plane orbital overlap driven by reduced in-plane disorder that affects the carrier mobility.

DOI: 10.1103/PhysRevB.95.064515

I. INTRODUCTION

Bismuth-based layered dichalcogenides have been drawing a large amount of attention due to their superconducting and thermoelectric properties [1–4]. Indeed, soon after the discovery of superconductivity in BiS_2-based systems [1,2], it was realized that not only do these materials have great potential in the field of new superconductors [3] but also they are likely candidates for materials with tunable thermoelectric properties [4] due to their low resistivity and low thermal conductivity [5]. The crystal structure of these materials is based on alternate stacking of electronically conducting BiS_2 layers and insulating block layers resembling that of CuO_2-based and FeAs/Se-based superconductors [6,7]. The parent phases of these dichalcogenides are semiconducting [1,8,9], and they become metallic, followed by superconductivity at low temperature, when electrons are doped in the BiS_2 layers with the dominant orbitals for the electron conduction being Bi $6p_{x,y}$. The doped systems show a wide range of superconducting transition temperature T_c with a maximum of ~10 K in the $LaO_{1-x}F_xBiS_2$ compound [3]. On the other hand, a relatively high thermoelectric performance (given by the dimensionless parameter $ZT = S^2T/\rho\kappa$, where S is the Seebeck coefficient, ρ is resistivity, and κ is thermal conductivity) has been found in the $LaOBiS_{2-x}Se_x$ system ($ZT \sim 0.36$ for LaOBiSSe at ~650 K) [10].

It is now becoming known that the carrier doping alone may not be sufficient to induce superconductivity in BiS_2-based compounds and their local structure optimization is required. This has been revealed by studies showing the highly susceptible and unstable nature of the BiS_2 lattice [11–16]. For instance, in-plane chemical pressure, which affects the local structure, is shown to be highly effective in controlling the superconducting properties of BiS_2-based compounds [17]. Indeed, in-plane chemical pressure can be tuned by an isovalent substitution, either in the REO (RE = rare earth) block layer in $REO_{0.5}F_{0.5}BiS_2$ [18–21] or by a direct substitution in the BiS_2 layer (e.g., Se substitution for S in $REO_{0.5}F_{0.5}BiS_{2-x}Se_x$ [22–25]). Indeed, the peculiar geometry of the BiS_2 layer with non-centrosymmetric distortion [11,14,15] is expected to control the physical properties of these materials.

Recently, a new BiS_2-based system, namely, $Eu_{0.5}La_{0.5}FBiS_{2-x}Se_x$, has been synthesized by codoping, which manifests bulk superconductivity by Se substitution [26]. The crystal structure is composed of $BiS_{2-x}Se_x$ conducting layers and $Eu_{0.5}La_{0.5}F$ block layers [see Fig. 1(b)]. The nominal carrier doping is 0.5 electron per Bi site, assuming that La^{3+} is substituting Eu^{2+}, with Ch (Ch = S, Se) being in the Ch^{2-} state. Figure 1(a) displays the superconductivity phase diagram of $Eu_{0.5}La_{0.5}FBiS_{2-x}Se_x$. For small Se substitution ($x = 0.0$ and 0.2), filamentary superconductivity with a lower transition temperature T_c is observed, while the bulk superconductivity appears for $x \geqslant 0.6$ [26]. Concomitantly, metallic conductivity appears for $x \geqslant 0.6$. Indeed, ρ_0 [shown in Fig. 1(a)], estimated from a linear fit of temperature-dependent resistivity $\rho(T)$ [26] in the interval of 250–300 K using the equation $\rho(T) = \rho_0 + AT$ (where A is a constant), shows a large drop for $x \leqslant 0.6$ in $Eu_{0.5}La_{0.5}FBiS_{2-x}Se_x$. These observations suggest that the electronic structure of the system is significantly affected by Se substitution.

In this work, we study the effect of Se substitution on the valence electronic states in $Eu_{0.5}La_{0.5}FBiS_{2-x}Se_x$. In particular, we investigate the Eu valence in $Eu_{0.5}La_{0.5}FBiS_{2-x}Se_x$ using x-ray absorption near-edge structure (XANES) spectroscopy and x-ray photoelectron spectroscopy (XPS) to address its possible role in the physical properties of the title system. XANES spectroscopy is a direct probe of the local structure and distribution of the valence electrons, with the final states in the continuum being due to multiple-scattering resonances [28]. We perform Eu L_3-edge XANES measurements that reveal a mixed valence of Eu (Eu^{2+} and Eu^{3+}) and its evolution with Se substitution. Eu $3d$ XPS also shows a similar trend of Eu valence as a function of Se content. Bi $4f$ XPS indicates that the effective electron carriers in the $BiCh_2$ layers are slightly increased (or unaffected) by Se substitution. On the basis of these results we discuss that the enhanced metallicity

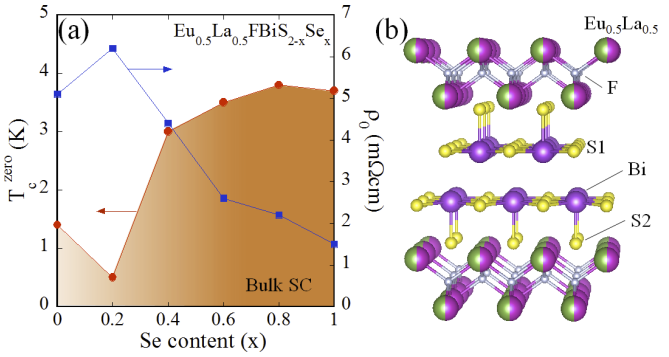

FIG. 1. (a) Superconductivity phase diagram of $Eu_{0.5}La_{0.5}FBiS_{2-x}Se_x$. The right axis shows ρ_0 estimated from a linear fit to the temperature-dependent resistivity [26] in the interval of 250–300 K using the equation $\rho(T) = \rho_0 + AT$, with A being a constant. (b) Crystal structure of $Eu_{0.5}La_{0.5}FBiS_{2-x}Se_x$ is schematically shown for $x = 0.0$. S1 and S2 denote the in-plane and the out-of-plane chalcogen sites. The crystal structure image was depicted using the VESTA program [27].

and superconductivity are not strictly related to Eu valence and should be associated with the enhanced carrier mobility caused by optimized in-plane orbital overlaps due to reduced disorder in the $BiCh_2$ layer.

II. EXPERIMENTAL DETAILS

The conventional solid-state reaction method was used to prepare polycrystalline samples of $Eu_{0.5}La_{0.5}FBiS_{2-x}Se_x$ ($x = 0.0$, 0.2, 0.4, 0.6, 0.8, and 1.0) [26]. The samples were characterized for their average structure using powder diffraction at the Xpress beamline of the Elettra synchrotron radiation facility, ensuring their phase purity. The samples with nominal $x = 0.0$, 0.2, 0.4, and 0.6 are single phase, while the samples with $x = 0.8$ and 1.0 contain a minor (13%) impurity phase of Bi_2Se_3. T_c was determined from the resistivity and magnetic susceptibility measurements [26].

X-ray absorption measurements at the Eu L_3 edge were performed using the BM08 beamline of the European Synchrotron Radiation Facility (ESRF) in Grenoble where the synchrotron radiation emitted by a bending magnet source was monochromatized with a double-crystal Si(311) monochromator. The measurements were made at room temperature in the transmission mode. The finely powdered samples of $Eu_{0.5}La_{0.5}FBiS_{2-x}Se_x$ were mixed uniformly in a boron nitride matrix and pressed into 13-mm-diameter pellets to obtain the edge jump, which was about 1. A similar procedure was used to prepare the $EuFBiS_2$ sample.

XPS measurements were performed on two single-phase samples ($x = 0.0$ and 0.6) at room temperature using the in-house UHV system at the Sapienza University of Rome, equipped with a double-anode XR50 x-ray source and an AR125 Omicron electron analyzer. The base pressure during the measurements was $\sim 6 \times 10^{-9}$ mbar. The Al $K\alpha$ emission line ($h\nu = 1486.6$ eV) was used to measure the Eu $3d$ XPS, while other core-level XPS measurements were acquired using the Mg $K\alpha$ emission line ($h\nu = 1253.6$ eV). Both the x-ray incident and photoelectron emission angles were $\sim 45^\circ$ for the

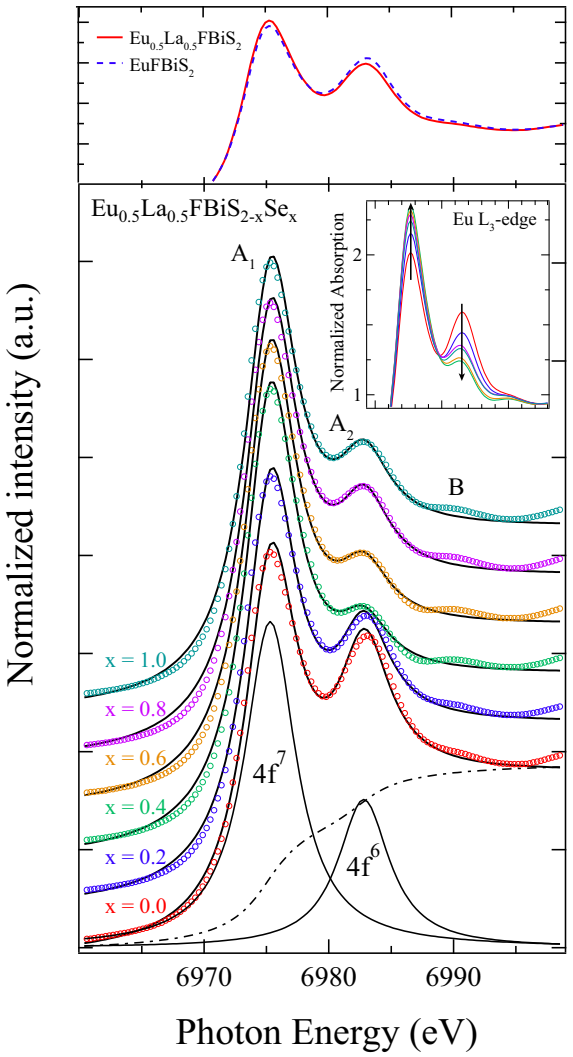

FIG. 2. (bottom) Eu L_3-edge normalized XANES spectra of $Eu_{0.5}La_{0.5}FBiS_{2-x}Se_x$. The spectra are shown deconvoluted (solid curves) in two Gaussian components corresponding to $4f^7$ (Eu^{2+}) and $4f^6$ (Eu^{3+}) after background (dash-dotted curve) removal. The inset shows a close-up of the Eu L_3-edge XANES white line peaks. (top) Eu L_3-edge XANES white line peaks of $EuFBiS_2$ (dashed line) are compared with those of $Eu_{0.5}La_{0.5}FBiS_2$ (solid line).

measurements. The sample surfaces were repeatedly scraped *in situ* by a diamond file to obtain clean surfaces.

III. RESULTS AND DISCUSSIONS

Figure 2 shows normalized Eu L_3-edge XANES spectra measured at room temperature on a series of $Eu_{0.5}La_{0.5}FBiS_{2-x}Se_x$ samples. The spectra are normalized with respect to the atomic absorption estimated by a linear fit to the high-energy part of the spectra. The L_3 absorption process is a $2p_{3/2} \rightarrow 5\epsilon d$ (or $2p_{3/2} \rightarrow 6\epsilon s$) transition governed by the dipole selection rules ($l = \pm 1$), and hence, empty states with d or s symmetries (and admixed $4f$ states) are reached in the final state. Since the probability of the $2p_{3/2} \rightarrow 6\epsilon s$ transition is relatively negligible compared with that of the $2p_{3/2} \rightarrow 5\epsilon d$ transition, the former can be ignored for describing the

L_3-edge XANES. In the present case, the Eu L_3-edge XANES spectra of $Eu_{0.5}La_{0.5}FBiS_{2-x}Se_x$ exhibit split white line in two peaks (peak A_1 at ~6975 eV and peak A_2 at ~6983 eV), corresponding to the transitions in the $4f^7$ and $4f^6$ final states, indicating the coexistence of Eu^{2+} and Eu^{3+} valences [29,30]. For $x = 0.0$, both Eu^{2+} and Eu^{3+} peaks are clearly observed, indicating the mixed-valence state of Eu, as shown earlier for $EuFBiS_2$ [31]. The Eu L_3-edge XANES spectrum measured on $EuFBiS_2$ is shown along with that of $Eu_{0.5}La_{0.5}FBiS_2$ for ready reference (top panel), comparing the two white line peaks, A_1 and A_2.

It is possible to estimate the average Eu valence by deconvolution of the Eu L_3-edge spectrum into Lorentzian components after substraction of the background estimated by an arctangent function for each spectral component (shown in Fig. 2). The average Eu valence, calculated from the ratio of the integrated intensity of the A_1 and A_2 peaks, is $\sim +2.31$ for $x = 0.0$. This is close to the Eu valence found earlier (in the range of +2.14 to 2.28) for $EuFBiS_2$ polycrystalline samples [31]. The Eu valence, estimated for $EuFBiS_2$ in the present work, is found to be $\sim +2.33$. This suggests that La^{3+} substitution, which is likely to generate electrons in the conducting BiS_2 layers, hardly affects the Eu valence. This already indicates that the Eu valence may not have a simple correlation with charge doping in the BiS_2 layer affecting the transport behavior of the title system.

On the other hand, the average valence seems to be largely affected by the Se substitution in the BiS_2 layer. This is evident from peak A_2 corresponding to $4f^6$ (Eu^{3+}), showing a suppressed intensity by Se substitution (see the inset of Fig. 2). In particular, for a sample with $x = 0.4$ and 0.6, the $4f^6$ peak is relatively weak. The evolution of the average Eu valence with Se substitution, estimated from the XANES spectra, is shown in Fig. 3(a). With increasing Se content, the average Eu valence decreases from $\sim +2.31$ (for $x = 0.0$) to $\sim +2.12$ (for $x = 0.4$), followed by a slight increase of up to $\sim +2.18$ for $x = 0.8$ and 1.0 samples.

It is worth noting that, in addition to the observed change in the A_1 and A_2 peaks (related to the change in the Eu valence) the weak feature B at ~6990 eV in the Eu L_3-edge XANES also reveals a systematic evolution. This feature is commonly observed in rare-earth L_3-edge XANES at ~20 eV above the main white line transition and is known to be highly sensitive to the intralayer and interlayer local geometry in layered systems [32,33]. The feature is also a marker sensitive to the electronic configuration of rare-earth atoms, and on the basis of multiple-scattering and density of states calculations it has been found that the feature B gains intensity with an increase in the $4f$ electron counts [33]. Here, the average number of $4f$ electrons increases with Se content (the ratio of $4f^7$ to $4f^6$ increases), which is consistent with the interpretation of the weak feature being due to a change in the electronic configuration of the rare-earth metal.

Coming back to the Eu valence, the mixed-valence state of Eu is also observed by core-level XPS measurements on the same samples. Figure 3(b) shows Eu $3d$ XPS for $x = 0.0$ and 0.6 samples. For both samples, two peaks corresponding to Eu^{2+} and Eu^{3+} states [34] can be seen. The average Eu valence is estimated from the ratio of the integrated intensity of these peaks after subtracting the Shirley-type backgrounds

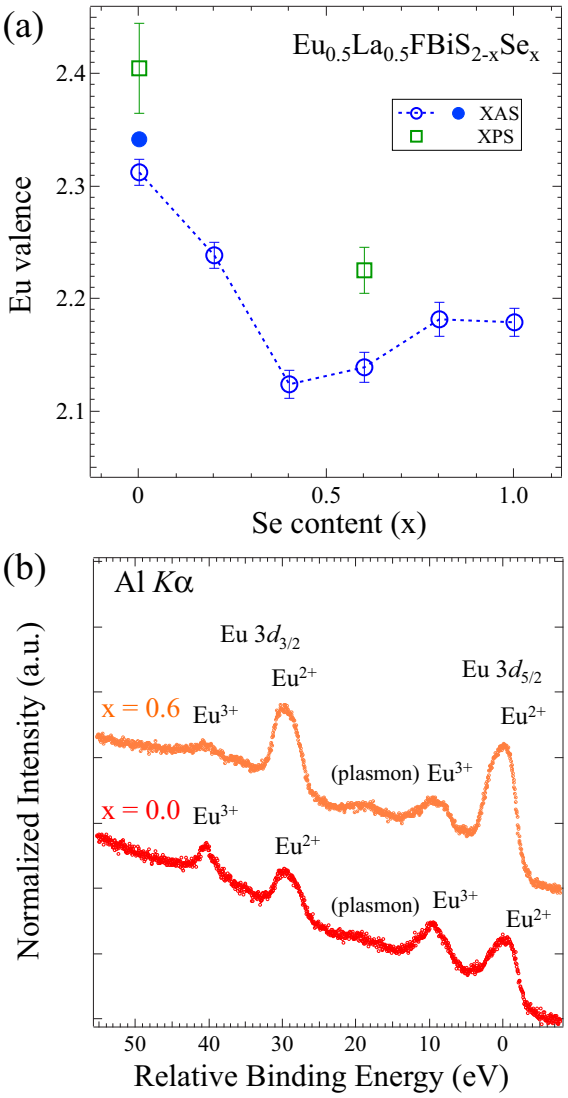

FIG. 3. (a) Eu valences estimated from XANES and XPS are shown as a function of Se substitution (solid circle corresponds to the valence of Eu for $EuFBiS_2$). (b) Eu $3d$ core-level XPS spectra of $Eu_{0.5}La_{0.5}FBiS_{2-x}Se_x$ for $x = 0.0$ and 0.6.

and is found to be $\sim +2.4$ and $\sim +2.2$ for $x = 0.0$ and 0.6, respectively. The estimated Eu valence from the XPS is also included in Fig. 3(a) together with the one estimated by the Eu L_3-edge XANES. Although the absolute values are slightly different, the tendency of the change in Eu valence by Se substitution is similar. The differences are likely to be due to different surface sensitivities of the XANES and XPS techniques. Therefore, we can conclude that the Eu valence in $Eu_{0.5}La_{0.5}FBiS_{2-x}Se_x$ decreases with increasing Se substitution, and hence, a smaller charge is available for a possible doping of the BiS_2 layer.

Further information on the impact of decreasing Eu valence on the BiS_2 layer with Se substitution in $Eu_{0.5}La_{0.5}FBiS_{2-x}Se_x$ can be obtained by Bi $4f$ XPS. Figure 4 shows Bi $4f$ core-level photoemission spectra of $x = 0.0$ and 0.6 samples, normalized to their integrated intensities. The spectra include S $2p$ and Se $3p$ signals, which are relatively weak because of the smaller photoemission cross section than that for Bi $4f$

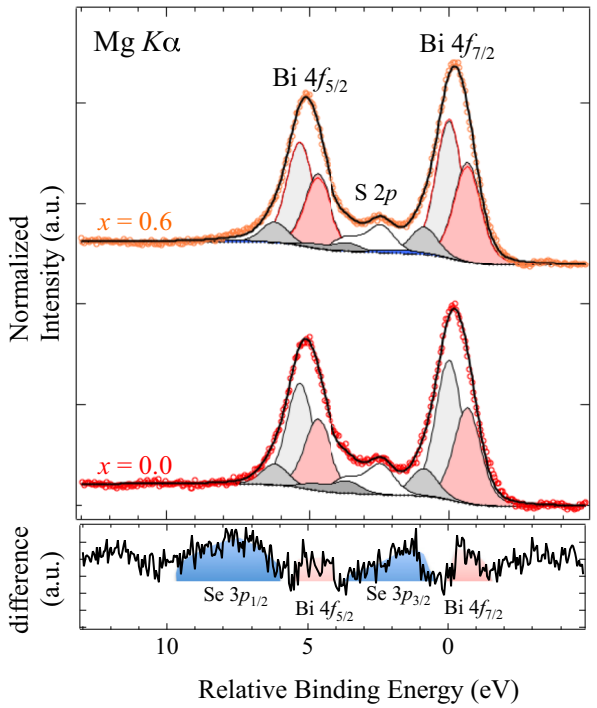

FIG. 4. The top panel shows Bi $4f$ core-level photoemission spectra of $Eu_{0.5}La_{0.5}FBiS_{2-x}Se_x$ for $x = 0.0$ and 0.6. The photoemission line shapes are deconvoluted in three components plus Ch components (S $3p$ and Se $4p$) after background subtraction (see text). The bottom panel shows the difference between the spectra for $x = 0.0$ and 0.6.

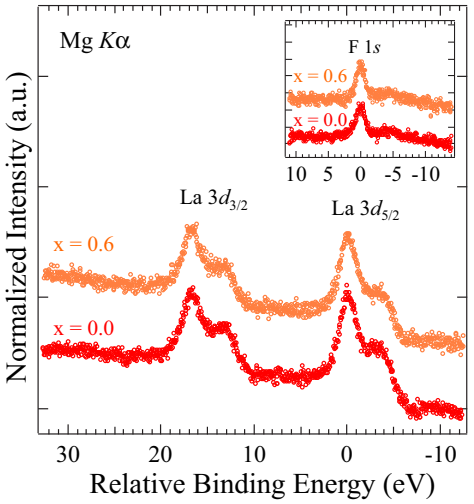

FIG. 5. La $3d$ core-level photoemission spectra of $Eu_{0.5}La_{0.5}FBiS_{2-x}Se_x$ for $x = 0.0$ and 0.6. F $1s$ XPS spectra for $x = 0.0$ and 0.6 are shown in the inset. In the F $1s$ spectra a broad Bi $4p_{3/2}$ feature is also included.

at the excitation energy used in this work [35]. In addition, the broadening due to the super-Coster-Kronig decay makes it difficult to distinguish the Se $3p$ signals in the $x = 0.6$ spectrum. In contrast to the large change observed in Eu $3d$ spectra (Fig. 3), the Bi $4f$ XPS spectra for the two samples reveal relatively small differences; that is, the chemical state of Bi remains almost similar in the two samples. The same can be said for La and F, which is apparent from the similarities of the La $3d$ and F $1s$ XPS spectra of the two samples displayed in Fig. 5, even though the La $3d$ and F $1s$ XPS spectra are relatively noisy due to the weak-photoemission cross section at the excitation energy used.

Since the superconductivity in BiS_2-based systems is known to be driven by charge carriers in the $BiCh_2$ layer, we have performed a detailed analysis of Bi $4f$ XPS measured on the two samples. A direct spectral difference between the two samples ($x = 0.6$ and $x = 0.0$) is shown in the bottom panel of Fig. 4. Broad weak structures (colored blue) in the higher-binding-energy region are due to Se $3p$, and sharper structures (colored pink) are due to Bi $4f$. The energy positions of the latter are slightly different from the Bi $4f$ peak position, suggesting the existence of multiple components in the Bi $4f$ spectra. Indeed, as shown in the top panel of Fig. 4, the XPS spectra are well reproduced by profile fitting using two Voigt functions, with a small component in the higher-binding-energy region likely to be due to the surface component or due to asymmetry of the main peaks. For the profile fits, the Gaussian widths are fixed to 0.97 eV, which corresponds to the total energy resolution of the Bi $4f$ XPS system used. The Lorentzian widths for the lower-binding-energy component (colored pink) are 0.26 eV, and those for the other components, including S $2p$, are 0.3 eV. The Shirley-type background was used. The spin-orbit splitting for Bi $4f$ and S $2p$ (5.3 and 1.2, respectively) and the branching ratios were set to their statistical values. The energy separation between the two Bi $4f$ main components is 0.65 eV, which is almost equal to that ($\sim$1 eV) reported for $LaO_{0.54}F_{0.46}BiS_2$ [36,37]. The relative binding energies for all components are fixed to the same values as those for $x = 0.0$, except for the Se $3p$, which does not exist in the $x = 0.0$ spectrum. The binding energy of the Se $3p$ is fixed to the one observed in the difference spectrum. The Gaussian and Lorentzian widths for Se $3p$ are 0.3 and 1.5 eV, respectively, the spin-orbit splitting is 5.8 eV, and the branching ratio is set to its statistical value. The black curves are the fit results.

The integrated relative intensity of the lower-binding-energy component (pink structure) for the Bi $4f$ peak increases by about 2% of the total under Se substitution. This increase is quantitatively consistent with the increased intensity observed in the difference spectrum. This small enhancement of the lower-energy component corresponds to an increase in the effective electrons at the Bi site in the $BiCh_2$ layer by Se substitution. Here, it is worth recalling that substitution of F in place of O ($LaO_{1-x}F_x$), known to increase charge density in the BiS_2 layer (of $LaO_{1-x}F_xBiS_2$), was studied earlier by Bi $4f$ XPS [37]. It has been found that the lower-energy component shows a systematic increase with electron doping in the BiS_2 layer through the substitution in the REO spacer layer. Therefore, the increase in the lower-energy spectral intensity of Bi $4f$ XPS with Se substitution indicates a small increase in the electron density. Because the average Eu valence is getting suppressed (the Eu^{3+} state is decreasing, as evident from both XANES and XPS measurements), the effective electrons in the $BiCh_2$ layers are expected to decrease if there is a charge transfer from the $Eu_{0.5}La_{0.5}F$ to the BiS_2

layer. This is inconsistent with the XPS results, which indicate a small increase in effective charge carriers. Therefore, other factors are expected to be active beyond the change in the effective charge in the $Eu_{0.5}La_{0.5}F$ layer.

Let us discuss the possible impact of the present results on the origin of the metallic character and superconductivity at low temperature in $Eu_{0.5}La_{0.5}FBiS_{2-x}Se_x$. First, $EuFBiS_2$ itself is expected to have excess electrons in the EuF layer due to the Eu mixed valence. In addition, enough electrons are doped in the $Eu_{0.5}La_{0.5}F$ layer by La^{3+} substitution (50%); however, the resistivity (for $x = 0.0$) shows that the sample is semiconducting. The system becomes metallic by Se substitution for $x \geqslant 0.6$. This implies that some other factors should interfere with the electron hopping in the BiS_2 layer. Because the BiS_2 layer in these materials is characterized by intrinsic noncentrosymmetric distortion [11–16], it is likely that this local disorder is renormalized with Se substitution in the system. Indeed, the high-symmetry BiS_2 lattice is instable [15,16], and the stable structure is characterized by different Bi-S distances within the BiS_2 plane. These distortions have been determined by pair distribution function [11] and extended x-ray-absorption fine structure studies [13,14]. The unstable nature of the BiS_2 lattice has also been indicated by diffraction studies revealing the easy transformability of the structure into tetragonal ($P4/nmm$) or monoclinic ($P21/m$) phases by substitution or pressure [11–14]. As a matter of fact, local structure distortions are found to decrease in a related compound, $LaOBiS_{2-x}Se_x$ [38], with a concomitant increase in carrier mobility as a function of Se substitution [39,40], determined to be due to enhanced in-plane orbital overlaps. A similar situation seems to occur in the present case in which the coexistence of phases with different structural symmetries characterized by their different local structures [15] gives rise to lower- and higher-energy components of the Bi $4f$ XPS due to smaller and larger distortions. Therefore, reduced local distortions enhancing the carrier mobility with Se substitution are the most plausible reason for the metallic character of $Eu_{0.5}La_{0.5}FBiS_{2-x}Se_x$. Reduced disorder also renormalizes electron-electron interactions, with increased electron mobility leading to screening of Coulomb repulsion and therefore increased superconductivity at low temperature.

IV. CONCLUSIONS

In summary, we have investigated valence electronic states of the layered $Eu_{0.5}La_{0.5}FBiS_{2-x}Se_x$ system using XANES and XPS spectroscopy. The results reveal that Eu in this system is in the mixed-valence state with coexisting Eu^{2+} and Eu^{3+}. The average valence shows a significant decrease with increasing Se substitution, revealed by both Eu L_3-edge XANES and Eu $3d$ XPS. This decrease in the Eu valence is expected to lead to a decrease in the electron carriers, unlike the Bi $4f$ XPS results revealing a small increase in the carrier density. From the combined analyses, we have discussed that Se substitution affects mainly the carrier mobility due to reduced local distortions. The reduced disorder in the $BiCh_2$ layer is expected to favor in-plane orbital overlaps, leading to increased carrier mobility and hence increased metallicity and superconductivity in $Eu_{0.5}La_{0.5}FBiS_{2-x}Se_x$.

ACKNOWLEDGMENTS

We thank ESRF staff for the assistance during the measurements. Y.M. would like to acknowledge hospitality at the Sapienza University of Rome. This work was partly supported by Grants-in-Aid for Scientific Research (Grants No. 15H05886, No. 16H04493, and No. 15H03691) and the Program for Promoting the Enhancement of Research University from MEXT and the Program for Advancing Strategic International Networks to Accelerate the Circulation of Talented Researchers from JSPS. The work is part of the executive protocol of the general agreement for cooperation between the Sapienza University of Rome and Tokyo Metropolitan University and that between the Sapienza University of Rome and Okayama University. The work at Sapienza is partially supported by PRIN2012 (Grant No. 2012X3YFZ2).

[1] Y. Mizuguchi, H. Fujihisa, Y. Gotoh, K. Suzuki, H. Usui, K. Kuroki, S. Demura, Y. Takano, H. Izawa, and O. Miura, Phys. Rev. B **86**, 220510 (2012).
[2] Y. Mizuguchi, S. Demura, K. Deguchi, Y. Takano, H. Fujihisa, Y. Gotoh, H. Izawa, and O. Miura, J. Phys. Soc. Jpn. **81**, 114725 (2012).
[3] Y. Mizuguchi, J. Phys. Chem. Solids **84**, 34 (2015).
[4] Y. Mizuguchi, A. Nishida, A. Omachi, and O. Miura, Cogent Phys. **3**, 1156281 (2016).
[5] A. Omachi, J. Kajitani, T. Hiroi, O. Miura, and Y. Mizuguchi, J. Appl. Phys. **115**, 083909 (2014).
[6] J. B. Bednorz and K. Müller, Z. Phys. B **64**, 189 (1986).
[7] Y. Kamihara, T. Watanabe, M. Hirano, and H. Hosono, J. Am. Chem. Soc. **130**, 3296 (2008).
[8] H. Usui, K. Suzuki, and K. Kuroki, Phys. Rev. B **86**, 220501 (2012).
[9] H. Usui and K. Kuroki, Novel Supercond. Mater. **1**, 50 (2015).
[10] A. Nishida, O. Miura, C.-H. Lee, and Y. Mizuguchi, Appl. Phys. Express **8**, 111801 (2015).
[11] A. Athauda, J. Yang, S. Lee, Y. Mizuguchi, K. Deguchi, Y. Takano, O. Miura, and D. Louca, Phys. Rev. B **91**, 144112 (2015).
[12] T. Sugimoto, B. Joseph, E. Paris, A. Iadecola, T. Mizokawa, S. Demura, Y. Mizuguchi, Y. Takano, and N. L. Saini, Phys. Rev. B **89**, 201117 (2014).
[13] E. Paris, B. Joseph, A. Iadecola, T. Sugimoto, L. Olivi, S. Demura, Y. Mizuguchi, Y. Takano, T. Mizokawa, and N. L. Saini, J. Phys. Condens. Matter **26**, 435701 (2014).
[14] Y. Mizuguchi, E. Paris, T. Sugimoto, A. Iadecola, J. Kajitani, O. Miura, T. Mizokawa, and N. L. Saini, Phys. Chem. Chem. Phys. **17**, 22090 (2015).
[15] Q. Liu, X. Zhang, and A. Zunger, Phys. Rev. B **93**, 174119 (2016).
[16] T. Yildirim, Phys. Rev. B **87**, 020506(R) (2013).
[17] Y. Mizuguchi, A. Miura, J. Kajitani, T. Hiroi, O. Miura, K. Tadanaga, N. Kumada, E. Magome, C. Moriyoshi, and Y. Kuroiwa, Sci. Rep. **5**, 14968 (2015).

[18] J. Kajitani, T. Hiroi, A. Omachi, O. Miura, and Y. Mizuguchi, J. Phys. Soc. Jpn. **84**, 044712 (2015).
[19] I. Jeon, D. Yazici, B. D. White, A. J. Friedman, and M. B. Maple, Phys. Rev. B **90**, 054510 (2014).
[20] G. S. Thakur, G. K. Selvan, Z. Haque, L. C. Gupta, S. L. Samal, S. Arumugam, and A. K. Ganguli, Inorg. Chem. **54**, 1076 (2015).
[21] Y. Fang, D. Yazici, B. D. White, and M. B. Maple, Phys. Rev. B **92**, 094507 (2015).
[22] T. Hiroi, J. Kajitani, A. Omachi, O. Miura, and Y. Mizuguchi, J. Phys. Soc. Jpn. **84**, 024723 (2015).
[23] A. K. Maziopa, Z. Guguchia, E. Pomjakushina, V. Pomjakushin, R. Khasanov, H. Luetkens, P. Biswas, A. Amato, H. Keller, and K. Conder, J. Phys. Condens. Matter **26**, 215702 (2014).
[24] X. C. Wang, D. Y. Chen, Q. Guo, J. Yu, B. B. Ruan, Q. G. Mu, G. F. Chen, and Z. A. Ren, arXiv:1404.7562.
[25] Y. Mizuguchi, T. Hiroi, and O. Miura, J. Phys. Conf. Ser. **683**, 012001 (2016).
[26] G. Jinno, R. Jha, A. Yamada, R. Higashinaka, T. D. Matsuda, Y. Aoki, M. Nagao, O. Miura, and Y. Mizuguchi, J. Phys. Soc. Jpn. **85**, 124708 (2016).
[27] K. Momma and F. Izumi, J. Appl. Crystallogr. **41**, 653 (2008).
[28] *X-ray Absorption: Principles, Applications, Techniques of EXAFS, SEXAFS, XANES*, edited by R. Prins and D. C. Koningsberger (Wiley, New York, 1988).
[29] H. Wada, A. Nakamura, A. Mitsuda, M. Shiga, T. Tanaka, H. Mitamura, and T. Goto, J. Phys. Condens. Matter **9**, 7913 (1997).
[30] A. P. Menushenkov, A. A. Yaroslavtsev, A. Y. Geondzhian, R. V. Chernikov, Y. V. Zubavichus X. Tan, and M. Shatruk, J. Supercond. Novel Magn. **28**, 995 (2015)
[31] H. F. Zhai, Z. T. Tang, H. Jiang, K. Xu, K. Zhang, P. Zhang, J. K. Bao, Y. L. Sun, W. H. Jiao, I. Nowik, I. Felner, Y. K. Li, X. F. Xu, Q. Tao, C. M. Feng, Z. A. Xu, and G. H. Cao, Phys. Rev. B **90**, 064518 (2014).
[32] Z. Wu, M. Benfatto, and C. R. Natoli, Phys. Rev. B **57**, 10336 (1998).
[33] W. Xu, A. Marcelli, B. Joseph, A. Iadecola, W. S. Chu, D. Di Gioacchino, A. Bianconi, Z. Y. Wu, and N. L. Saini, J. Phys. Condens. Matter **22**, 125701 (2010).
[34] B. T. Thole, G. van der Laan, J. C. Fuggle, G. A. Sawatzky, R. C. Karnatak, and J.-M. Esteva, Phys. Rev. B **32**, 5107 (1985).
[35] J. J. Yeh and I. Lindau, At. Data Nucl. Data Tables **32**, 1 (1985).
[36] K. Terashima, J. Sonoyama, T. Wakita, M. Sunagawa, K. Ono, H. Kumigashira, T. Muro, M. Nagao, S. Watauchi, I. Tanaka, H. Okazaki, Y. Takano, O. Miura, Y. Mizuguchi, H. Usui, K. Suzuki, K. Kuroki, Y. Muraoka, and T. Yokoya, Phys. Rev. B **90**, 220512 (2014).
[37] S. Nagira, J. Sonoyama, T. Wakita, M. Sunagawa, Y. Izumi, T. Muro, H. Kumigashira, M. Oshima, K. Deguchi, H. Okazaki, Y. Takano, O. Miura, Y. Mizuguchi, K. Suzuki, H. Usui, K. Kuroki, K. Okada, Y. Muraoka, and T. Yokoya, J. Phys. Soc. Jpn. **83**, 033703 (2014).
[38] E. Paris, Y. Mizuguchi, M. Y. Hacisalihoglu, T. Hiroi, B. Joseph, G. Aquilanti, O. Miura, T. Mizokawa, and N. L. Saini, J. Phys. Condens. Matter (2017), doi:10.1088/1361-648X/aa5e97.
[39] A. Nishida, H. Nishiate, C. H. Lee, O. Miura, and Y. Mizuguchi, J. Phys. Soc. Jpn. **85**, 074702 (2016).
[40] Y. Mizuguchi, A. Miura, A. Nshida, O. Miura, K. Tadanaga, N. Kumada, C. H. Lee, E. Magome, C. Moriyoshi, and Y. Kuroiwa, J. Appl. Phys. **119**, 155103 (2016).